Magnetic Resonance Imaging 117 (2025) 110328

Contents lists available at ScienceDirect

Magnetic Resonance Imaging

journal homepage: www.elsevier.com/locate/mri

Log subtracted inversion recovery

Mark Bydder [a,*], Daniel M. Cornfeld [a,b], Tracy R. Melzer [c,d,e], Paul Condron [a,b], Gil Newburn [a], Eryn E. Kwon [a,b,f], Maryam Tayebi [a,b], Miriam Scadeng [b,f], Samantha J. Holdsworth [a,b], Graeme M. Bydder [a,g]

[a] Mātai Medical Research Institute, Tairāwhiti, Gisborne, New Zealand
[b] Department of Anatomy & Medical Imaging, Faculty of Medical and Health Sciences & Centre for Brain Research, University of Auckland, New Zealand
[c] Department of Medicine, University of Otago, Christchurch 8011, New Zealand
[d] New Zealand Brain Research Institute, Christchurch 8011, New Zealand
[e] Te Kura Mahi ā-Hirikapo, School of Psychology, Speech and Hearing, University of Canterbury, Christchurch 8140, New Zealand
[f] Auckland Bioengineering Institute, Auckland, New Zealand
[g] Department of Radiology, University of California San Diego, San Diego, CA, USA

ARTICLE INFO

Keywords:
MP2RAGE
FLAWS
dSIR
Inversion recovery
T1 mapping

ABSTRACT

Magnetic resonance imaging (MRI) techniques have recently been developed for obtaining high T_1 contrast images using inversion recovery (IR) images at two inversion times (TIs) rather than a single TI. They use simple mathematical operations – multiplication, addition, subtraction, division – to create images not attainable by conventional IR. The present study describes a novel two-point IR technique formed by the subtraction of log images. Results show it has a near-linear response to T_1 between the nullpoints that peaks sharply at the nullpoints. This produces a bright isoT_1 contour at interfaces between tissues where partial volume mixing generates specific T_1s. This can provide anatomical information in areas where the signal is not well-differentiated on conventional images.

1. Introduction

Several imaging techniques based on inversion recovery (IR) have recently been developed to generate nonlinear T_1 contrasts with suppression and/or amplification of specific T_1s. These include *Magnetization Prepared 2 Rapid Acquisition Gradient Echo* (MP2RAGE) [1], *FLuid And Water Suppression-high contrast* (FLAWS-hc) [2] and *divided Subtracted IR* (dSIR) [3]. Contrast is produced by subtracting, adding, dividing and/or multiplying images with different inversion times (TIs) rather than relying on the physical evolution of the signal to produce contrast in a single TI, as with conventional IR techniques.

The MP2RAGE and FLAWS-hc techniques typically use a wide separation between the TIs, which gives a broad T_1 response, while the dSIR is more focused on a narrow *middle Domain* (mD) between the nullpoints. A feature of dSIR is that T_1s inside the mD are mapped between ±1, which provides high dynamic range, while those outside the mD are mapped towards zero. Clinical studies report changes seen with dSIR in mild traumatic brain injury (mTBI), hypoxic injury, substance abuse and ischemic leukoencephalopathy that are not seen with conventional sequences [4].

Letting M_1 and M_2 represent the magnitude images at different TIs, the dSIR image is formed by Eq. 1.

$$\mathrm{dSIR} = \frac{M_1 - M_2}{M_1 + M_2} \tag{1}$$

As the separation of the TIs (ΔTI) approaches zero the equation becomes a differential

$$\mathrm{dSIR} \rightarrow \frac{dM}{2M} = \frac{1}{2} d\mathit{ln}(M) \tag{2}$$

which for the IR signal model $M = 1 - 2e^{-TI/T_1}$ has the functional form of Eq. 3.

$$\frac{\partial \mathit{ln}(M)}{\partial TI} = \frac{2}{(e^{TI/T_1} - 2)T_1} \tag{3}$$

* Corresponding author.
E-mail addresses: markbydder@gmail.com (M. Bydder), d.cornfeld@matai.org.nz (D.M. Cornfeld), tracy.melzer@otago.ac.nz (T.R. Melzer), p.condron@matai.org.nz (P. Condron), g.newburn@matai.org.nz (G. Newburn), e.kwon@matai.org.nz (E.E. Kwon), m.tayebi@matai.org.nz (M. Tayebi), m.scadeng@auckland.ac.nz (M. Scadeng), s.holdsworth@matai.org.nz (S.J. Holdsworth), gbydder@health.ucsd.edu (G.M. Bydder).

https://doi.org/10.1016/j.mri.2025.110328
Received 6 November 2024; Received in revised form 7 January 2025; Accepted 11 January 2025
Available online 16 January 2025

This represents the fractional change in IR signal with TI. When the signal crosses zero the fractional change exhibits extreme variation over a narrow T_1 domain, as indicated in Fig. 1 (left).

The practical use of this type of contrast is limited. However by replacing the derivative with a finite difference the poles are separated to give the same transition over a wider T_1 domain (Fig. 1, right). This suggests a new variant of dSIR formed from the difference of log images and is referred to as *log subtracted inversion recovery* (lSIR) in the present study.

$$\text{lSIR} \equiv \frac{1}{2}ln(M_1) - \frac{1}{2}ln(M_2) \tag{4}$$

The T_1 response of lSIR is shown in Fig. 2 compared to dSIR. The relation between the two can be expressed as the inverse hyberbolic tangent, i.e. lSIR = atanh(dSIR) (see Appendix).

Based on an understanding of contrast as slope versus T_1, the lSIR has highly elevated contrast at the nullpoints relative to dSIR. When the upper nullpoint is intermediate between two tissues with distinct T_1s – e.g. white and gray matter – this can greatly enhance the ability to resolve features at the interface. As the partial volume fraction (η) transitions from 0 to 1 (i.e. white to gray matter), the mixture exhibits intermediate T_1 values associated with the sharp filter response. A simple approximation is to model $1/T_1$ as linear in η [5].

$$\frac{1}{T_1} = \frac{1-\eta}{T_1(\text{white})} + \frac{\eta}{T_1(\text{gray})} \tag{5}$$

Uncertainty in T_1(white) and T_1(gray), as well as imperfect knowledge of the relaxation model, makes it difficult to associate the peak with an exact value of η, however images show a bright isoT$_1$ contour that corresponds to a specific voxel composition. This can be a useful as a de facto tissue boundary, or to identify subtle T_1 differences in tissues.

The present study introduces and demonstrates the lSIR technique as a novel variant of dSIR that enhances specific T_1 values to improve visualization at tissue boundaries and in partial volume mixtures.

2. Methods

The study was conducted in accordance with the Declaration of Helsinki and approved by the Auckland Hospital Research Ethics Committee (approval number AHRECAH1006 in 2021). Informed consent was obtained from all subjects whose images are used in this manuscript.

MRI scans were performed on a normal volunteer and a patient with mTBI using a General Electric Premier 3 T scanner: 2D IR fast spin echo, repetition time 9000 ms, echo time 12 ms, echo train length 10, flip angle 150°, no. slices 35, slice thickness 4 mm, matrix 256 [2], field of view 256 mm, bandwidth 260 Hz/pixel, parallel acceleration factor 2. Two separate acquisitions were performed at TI = 350 ms and 500 ms with a total scan time of 230 s.

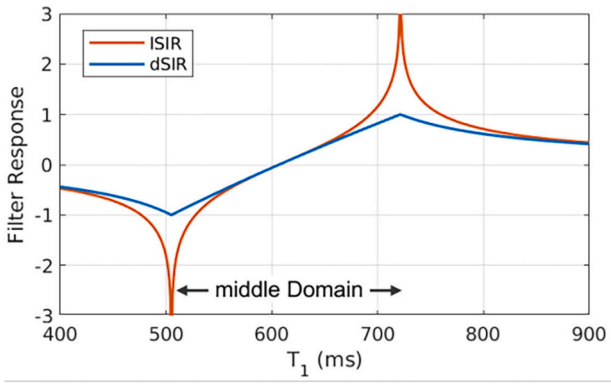

Fig. 2. The T_1 response of lSIR (red) and dSIR (blue) filters. The bipolar shape of the dSIR is amplified in the vicinity of the nullpoints. In this example the nullpoints were chosen to be 505 and 722 ms, corresponding to TIs of 350 and 500 ms. (For interpretation of the references to colour in this figure legend, the reader is referred to the web version of this article.)

Images were retrieved from the scanner in DICOM format for offline processing in MATLAB 2023a (The Mathworks, Natick MA). The dSIR and lSIR were produced from magnitude images. If signed or complex images are used, the real part contains the lSIR image and the imaginary part contains the phase difference between the two TI images.

3. Results

An example from the normal volunteer is shown in Fig. 3. Since dSIR signal is between ±1 and lSIR requires a larger number of grayscales, the dSIR images are shown with two window/level settings to allow unbiased comparison.

The images show that lSIR exhibits many regions with enhanced clarity relative to dSIR. While the image appears to be edge-enhanced, the edge is specific only to a single $T_{1\ \text{value}}$. It can be interpreted physically as representing a specific volume fraction of white matter and gray matter (nominally 50 %).

Figure 4 shows a zoomed detail of the images in Fig. 3. The isoT$_1$ contour highlights a boundary along which the partial volume fraction is constant, i.e. voxels either side are either $< \eta$ or $> \eta$. This helps to define the boundary between white matter and gray matter in regions of the image that are indistinct. The boundaries are much more obvious on the lSIR image than the dSIR.

An example from a patient with mTBI is shown in Fig. 5. The patient has elevated T_1s in white matter which appear at the top of the dynamic range in the dSIR image. The lSIR image reveals that the T_1 crosses the

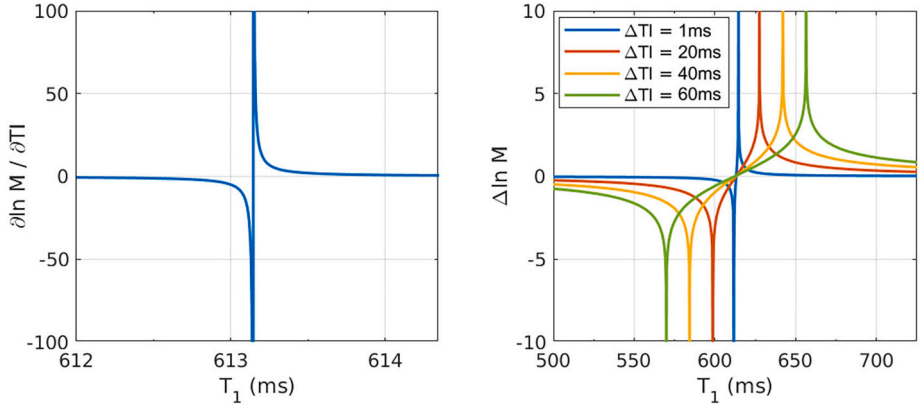

Fig. 1. Plot (left) shows the fractional change in IR signal as the signal crosses zero (Eq. 3). The curve has extreme sensitivity to T_1 over a narrow domain. By using a finite ΔTI instead of a derivative, the poles are separated to give the same transition over a wider T_1 domain (right).

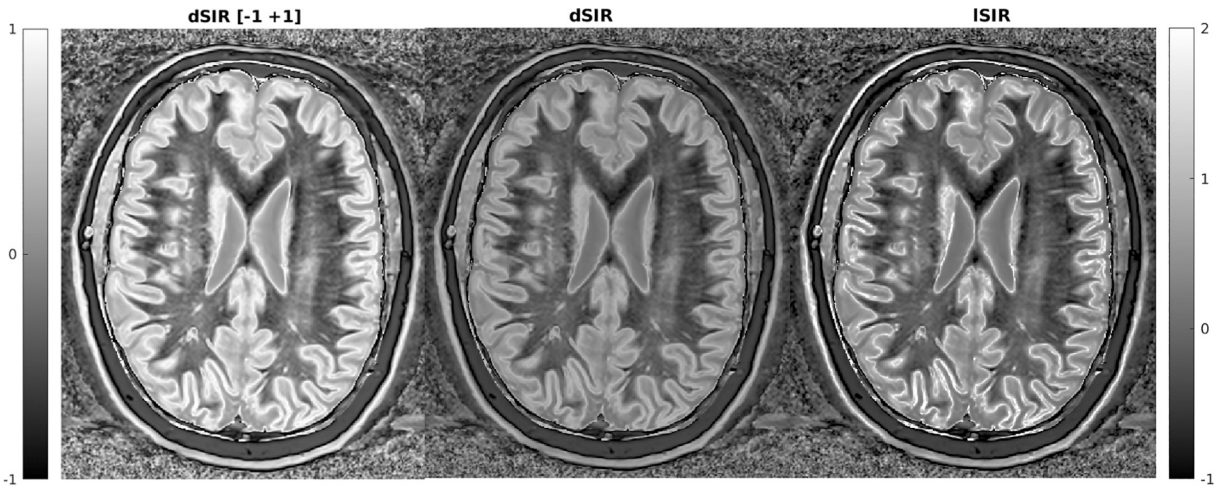

Fig. 3. Comparison of dSIR (left/center) and lSIR (right) images in the normal volunteer. To ensure a fair comparison the dSIR is shown with two colorbar settings since the lSIR image requires additional grayscale levels. In all images white matter appears low signal (black) providing a background against which structures with slightly longer T_1s appear mid-gray. At the boundary between white matter and gray matter, the image intensity reaches a maximum at a T_1 intermediate between those of white and gray matter.

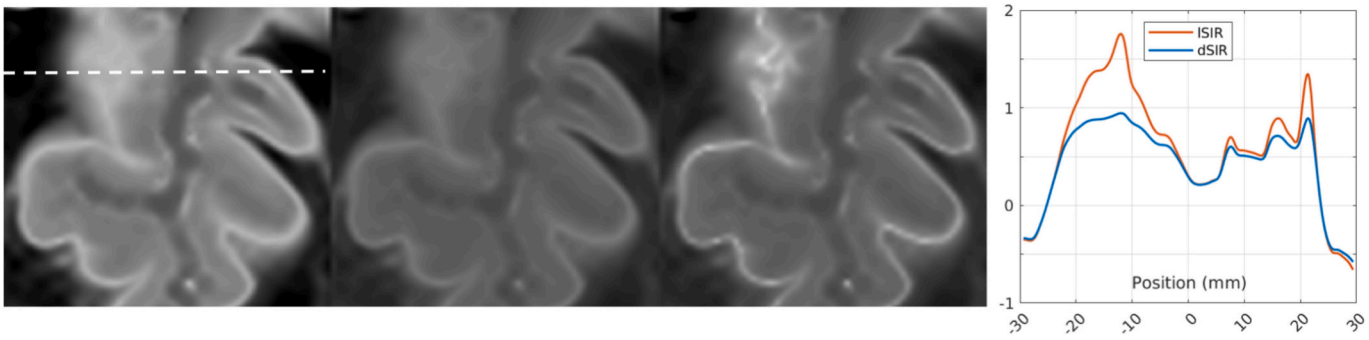

Fig. 4. Detail of Fig. 3 illustrating the ability of lSIR to clarify morphology at tissue boundaries. Compared with the dSIR images (left and center), the lSIR (right) reveals structures that are present but hidden in a grayscale of similar intensities. The line-plot shows the intensity variation across the image (indicated by dashed line in the left image). There is no simple window/level that can align the blue and red lines. (For interpretation of the references to colour in this figure legend, the reader is referred to the web version of this article.)

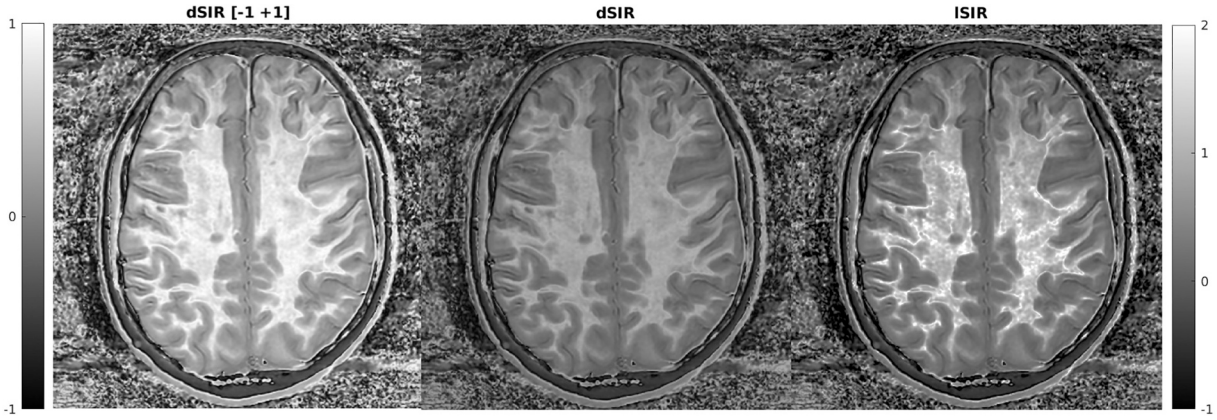

Fig. 5. Comparison of dSIR and lSIR images in a patient with mTBI in which the T_1 of white matter equals or exceeds the upper nullpoint. The lSIR image provides higher precision at the boundary with gray matter and shows structured changes in white matter. These changes are present on the dSIR image but are more obvious on the lSIR image.

mD in numerous places; since only a narrow range of T_1s give the sharp signal response, it is likely these are generated by a partial volume effect which implies there are tissues with different T_1s within the white matter. These contours may represent a complex interface between tissues formed by specific partial volume mixtures. The tissues involved are not necessarily white matter and gray matter but rather micro-structural white matter alterations due to edema, inflammation and/or demyelination. The presence of such features shows that the diffuse

white matter dSIR signal elevation reported in patients [4] may contain discernable structures.

4. Discussion

The difference of log images is in some ways a natural way to look at MR images. This can be understood more easily for TE, where the difference of log images is proportional to $1/T_2$, but also for TI where the difference of log images is (almost) proportional to T_1. Specifically, it is a bipolar-filtered T_1 map that is linear at the center of the mD and has nonlinear amplification at the nullpoints. This produces a bright contour at the interface between tissues where partial volume mixtures generate T_1s associated with the asymptote of the atanh filter.

Log subtraction is additive for multiple contrast types so if M_1 and M_2 are acquired with different TEs as well as different TIs then the difference of logs becomes lSIR $\pm \Delta TE/2T_2$ where the T_1 information is in the first term and the T_2 information in the second term. Mixed contrast filters can be tuned to emphasize specific tissue property combinations.

Noise amplification may be expected around the peak of the lSIR filter, however this is mitigated by the reduction of standard deviation of rectified noise close to zero. Infinities due to log(0) or atanh(±1) are implicitly regularized by noise bias in the image [6] but may be explicitly avoided by using similar filters that are well-behaved, e.g. dSIR + $\frac{1}{3}$dSIR^3, which is the 2-term Taylor expansion of atanh. Filters may be applied to T_1 maps obtained by other techniques, however results may vary if the TIs are substantially different or if another method of T_1 estimation was used. Although T_1 represents a specific tissue property (spin-lattice relaxation) it is often measured in samples where there is exchange between heterogeneous pools in unequal initial magnetization states, under varying degrees of RF irradiation, using data blended from multiple time-points during the recovery [7–10]. Furthermore, not all tissues exchange magnetization, or may exhibit complicated relaxation behavior in mixtures [11]. Distinguishing monoexponential, biexponential or other behavior is not possible with two data points, although this is not necessary for lSIR to amplify boundaries. The interpretation of the boundary as a specific partial volume fraction *is* model-dependent and this is also limited by uncertainty in the T_1 values [12]. Tissue boundaries are affected by susceptibility, chemical shift and point spread function contamination, which may complicate interpretation.

In conclusion, the present study has described an ultrahigh contrast technique for enhancing signal at tissue interfaces. In vivo results sharpen the white matter-gray matter boundary and provide additional clarity in regions of indistinct signal.

CRediT authorship contribution statement

Mark Bydder: Writing – original draft, Investigation, Formal analysis, Conceptualization. **Daniel M. Cornfeld:** Software, Investigation, Conceptualization. **Tracy R. Melzer:** Investigation. **Paul Condron:** Resources, Methodology, Investigation. **Gil Newburn:** Supervision. **Eryn E. Kwon:** Investigation, Conceptualization. **Maryam Tayebi:** Validation, Data curation. **Miriam Scadeng:** Resources, Investigation. **Samantha J. Holdsworth:** Investigation, Funding acquisition. **Graeme M. Bydder:** Writing – review & editing, Resources, Project administration.

Declaration of competing interest

None.

Acknowledgements

This research was funded by the Fred Lewis Enterprise Foundation, the Hugh Green Foundation, the JN & HB Williams Foundation, the Mangatawa Beale Williams Memorial Trust, Anonymous Donor, an Agility Grant from the Wu Tsai Human Performance Alliance, Friends of Mātai Blue Sky Fund, and Kānoa—Regional Economic Development & Investment Unit of New Zealand. We are also grateful for support from GE Healthcare and Mātai Ngā Māngai Māori.

Appendix A

The inverse hyperbolic tangent obeys the following trigonometric identity [13]

$$\operatorname{atanh}(x) = \frac{1}{2} ln\left(\frac{1+x}{1-x}\right)$$

which can be rewritten as $\frac{1}{2}ln(1+x) - \frac{1}{2}ln(1-x)$. Substituting argument x with dSIR (Eq. 1) yields

$$\frac{1}{2} ln\left(1+\frac{M_1-M_2}{M_1+M_2}\right) - \frac{1}{2} ln\left(1-\frac{M_1-M_2}{M_1+M_2}\right).$$

The terms in parentheses may be collected over a common divisor to give

$$\frac{1}{2} ln\left(\frac{2M_1}{M_1+M_2}\right) - \frac{1}{2} ln\left(\frac{2M_2}{M_1+M_2}\right)$$

which expands to

$$\frac{1}{2} ln(2) + \frac{1}{2} ln(M_1) - \frac{1}{2} ln(M_1+M_2) - \frac{1}{2} ln(2) - \frac{1}{2} ln(M_2) + \frac{1}{2} ln(M_1+M_2).$$

Most of the terms cancel to leave the final result: $\operatorname{atanh}(\text{dSIR}) = \frac{1}{2}ln(M_1) - \frac{1}{2}ln(M_2)$.

The effect on contrast, i.e. the ability to discriminate tissues with similar T_1s, can be calculated by taking the derivative with respect to T_1. Based on the linear approximation of dSIR inside the mD [6] and the derivative of atanh [13] the following is obtained:

$$\frac{d(\text{lSIR})}{dT_1} \approx \left(T_1 - \frac{TI_1}{ln2}\right)^{-1} \left(T_1 - \frac{TI_2}{ln2}\right)^{-1} \frac{ln4}{\Delta TI}$$

This shows that lSIR has the same overall slope as dSIR but with poles at the nullpoints.

References

[1] Marques JP, Kober T, Krueger G, van der Zwaag W, Van de Moortele P-F, Gruetter R. MP2RAGE, a self bias-field corrected sequence for improved segmentation and T_1-mapping at high field. NeuroImage 2010;49:1271–81.

[2] Beaumount J, Saint-Jalmes H, Acosta O, Kober T, Tanner M, Ferre JC, et al. Multi T1-weighted contrast MRI with fluid and white matter suppression at 1.5T. Magn Reson Imaging 2019;63:217–25.

[3] Ma YJ, Moazamian D, Cornfeld DM, Condron P, Holdsworth SJ, Bydder M, et al. Improving the understanding and performance of clinical MRI using tissue property filters and the central contrast theorem, MASDIR pulse sequences and synergistic contrast MRI. Quant Imaging Med Surg 2022;12:4658–90.

[4] Cornfeld D, Condron P, Newburn G, McGeown J, Scadeng M, Bydder M, et al. Ultra-high contrast MRI: using divided subtracted inversion recovery and divided echo subtraction sequences to study the brain and musculoskeletal system. Bioengineering 2024;11:441.

[5] Zimmerman JR, Brittin WE. Nuclear magnetic resonance studies in multiple phase systems: lifetime of a water molecule in an adsorbing phase on silica gel. Phys Chem 1957;6:1328–33.

[6] Bydder M, Ali F, Condron P, et al. Validation of an ultrahigh contrast divided subtracted inversion recovery technique using a standard T_1 phantom. NMR Biomed 2024:e5269.

[7] Rioux JA, Levesque IR, Rutt BK. Biexponential longitudinal relaxation in white matter: characterization and impact on T_1 mapping with IR-FSE and MP2RAGE. Magn Reson Med 2016;75:2265–77.

[8] Keenan KE, Tasdelen B, Javed A, et al. T_1 and T_2 measurements across multiple 0.55T MRI systems using open-source vendor-neutral sequences. Magn Reson Med 2025;93:289–300.

[9] Hajnal JV, Baudouin CJ, Oatridge A, Young IR, Bydder GM. Design and implementation of magnetisation transfer pulse sequences for clinical use. J Comput Assist Tomogr 1992;16(1):7–18.

[10] Reynolds LA, Morris SR, Vavasour IM, et al. Nonaqueous magnetization following adiabatic and selective pulses in brain: T_1 and cross-relaxation dynamics. NMR Biomed 2023;36:e4936.

[11] Hu HH, Nayak KS. Change in the proton T_1 relaxation time of fat and water in mixture. Magn Reson Med 2010;63:494–501.

[12] Wright PJ, Mougin OE, Totman JJ, et al. Water proton T_1 measurements in brain tissue at 7, 3, and 1.5T using IR-EPI, IR-TSE, and MPRAGE: results and optimization. Magn Reson Mater Phy 2008;21:121 (Table 2).

[13] Jeffrey A. Mathematics for engineers and scientists. 6th ed. Chapman and Hall/CRC; 2005. p. 324–6.